IMMUNOLOGY

Engineered probiotics biofilm enhances osseointegration via immunoregulation and anti-infection

Lei Tan[1]*, Jieni Fu[2]*, Fan Feng[1]*, Xiangmei Liu[1†], Zhenduo Cui[2], Bo Li[3], Yong Han[3], Yufeng Zheng[4], Kelvin Wai Kwok Yeung[5], Zhaoyang Li[2], Shengli Zhu[2], Yanqin Liang[2], Xiaobo Feng[6], Xianbao Wang[1], Shuilin Wu[2†]

Preventing multidrug-resistant bacteria–related infection and simultaneously improving osseointegration are in great demand for orthopedic implants. However, current strategies are still limited to a combination of non–U.S. Food and Drug Administration–approved antibacterial and osteogenic agents. Here, we develop a food-grade probiotic–modified implant to prevent methicillin-resistant *Staphylococcus aureus* (MRSA) infection and accelerate bone integration. *Lactobacillus casei* is cultured on the surface of alkali heat–treated titanium (Ti) substrates and inactivated by ultraviolet irradiation to avoid sepsis induced by viable bacteria. This inactivated *L. casei* biofilm shows excellent 99.98% antibacterial effectiveness against MRSA due to the production of lactic acid and bacteriocin. In addition, the polysaccharides in the *L. casei* biofilm stimulate macrophages to secrete abundant osteogenic cytokines such as oncostatin M and improve osseointegration of the Ti implant. Inactivated probiotics modification can be a promising strategy to endow implants with both excellent self-antibacterial activity and osteointegration ability.

INTRODUCTION

Implant-related infections and insufficient osteogenic activity can cause the failure of the implant or delay the recovery of patients. The subsequent financial burden and physical pain become unavoidable (*1*). In particular, fracture incidence is very high in the elderly due to their osteoporosis (*2*). After undergoing fracture surgery, the elderly patients often suffer from cardiovascular diseases such as thrombus formation and subsequent myocardial infarction due to delayed healing and long periods of bed rest, which increase the mortality of aged patients (*3*, *4*). In addition, to prevent bacterial infection, the patients generally receive systemic antibiotics treatment after orthopedic surgery. However, the increasing incidence of multidrug-resistant bacterial infections has seriously threatened human health due to the overuse or misuse of antibiotics (*5*). The inability of existing antibiotics to treat all superbacteria-associated infections is already becoming a very serious problem.

Therefore, an ideal implant should have desirable biofunctions to accelerate bone tissue regeneration and prevent drug-resistant bacterial infections simultaneously. To address this issue, different strategies have been attempted to integrate both antibacterial and osteogenic properties into the implant, incorporating materials such as organic antibacterial agents or antibiotics with osteogenic peptides or growth factors (*6*), and Ag/Zn (*7*), Ag/Sr (*8*), Cu/Mg (*9*), or ZnO/osteogenic peptides (*10*). Current strategies employ elaborate fabrication processes or use heavy metals with potential tissue toxicity, which may hinder their clinical potential (*11*). Therefore, it is highly desirable to develop a simple and safe strategy to prevent bacterial infection and improve tissue regeneration, especially using U.S. Food and Drug Administration–approved materials.

Microbial-mediated treatments have attracted wide attention for various diseases. For cancer therapy, some bacteria such as *Salmonella*, *Escherichia*, and *Listeria* show targeting ability to the hypoxic microenvironment of tumor tissues (*12*). Nonpathogenic bacteria can be genetically programmed or combined with nanomaterials to suppress tumor growth (*13*, *14*). Probiotics play an important role in the gut microbiome, which can maintain healthy bowels. As nonpathogenic organisms, probiotics are widely used for many digestive diseases such as inflammatory bowel disease, irritable bowel syndrome, and infectious diarrhea, because of their ability to eliminate pathogenic bacteria and regulate the host immune system (*15*). Probiotics also can be designed to produce functional compounds or proteins to ameliorate inflammatory diseases or improve tissue regeneration (*16*, *17*). Despite the sky-is-the-limit potential of those genetically programmed bacteria, their clinical applications have been limited by the potential problem of biosafety induced by off-target toxicity (*18*). In addition, most probiotics must be administered orally because of the risk of bacteremia (*19*) or sepsis (*20*) when viable bacteria are introduced into the bloodstream. *Lactobacillus casei*, as resident probiotics in the human intestine and mouth, can be found in dairy foods such as yogurt and cheese (*21*). It is well known that *L. casei* shows excellent antibacterial performance against pathogenic bacteria, including methicillin-resistant *Staphylococcus aureus* (MRSA), due to the production of bacteriocin, lactic acid, and hydrogen peroxide (*22*, *23*). However, considering the potential risk of sepsis, its use in the prevention of implant-related infections by MRSA remains underexplored.

[1]Ministry of Education Key Laboratory for the Green Preparation and Application of Functional Materials, Hubei Key Laboratory of Polymer Materials, School of Materials Science and Engineering, Hubei University, Wuhan 430062, China. [2]School of Materials Science and Engineering, the Key Laboratory of Advanced Ceramics and Machining Technology by the Ministry of Education of China, Tianjin University, Tianjin 300072, China. [3]State Key Laboratory for Mechanical Behavior of Materials, School of Materials Science and Engineering, Xi'an Jiaotong University, Xi'an, Shaanxi 710049, China. [4]State Key Laboratory for Turbulence and Complex System and Department of Materials Science and Engineering, College of Engineering, Peking University, Beijing 100871, China. [5]Department of Orthopaedics and Traumatology, Li Ka Shing Faculty of Medicine, The University of Hong Kong, Pokfulam, Hong Kong, China. [6]Department of Orthopaedics, Union Hospital, Tongji Medical College, Huazhong University of Science and Technology, Wuhan 430022, China.
*These authors contributed equally to this work.
†Corresponding author. Email: liuxiangmei1978@163.com (X.L.); shuilin.wu@gmail.com (S.W.)

Moreover, the cell walls of probiotic bacteria contain components such as peptidoglycan, lipoteichoic acid, and some specific proteins, which play prominent roles in modulation of the human immune system (*24*). As we know, implantation of biomaterials generates an initial inflammatory response. During the foreign body reaction, host macrophages abundantly accumulate on the surface of implants (*25*). The activity of macrophages plays a crucial role in modulating the balance between inflammation and regeneration. Macrophages can be stimulated to produce osteogenic factors to accelerate bone integration with the implant (*26–28*). Polysaccharides such as lipopolysaccharide can activate macrophages through binding of sugar units to carbohydrate receptors on the macrophage surface (*29*, *30*). A recent study has reported the use of zymosan, a fungal polysaccharide, to modify the surface of Ti implants, and thus improve implant-bone integration through activating macrophages to secrete osteogenic cytokines (*31*). It is known that bacterial biofilms are composed mainly of bacteria and the surrounding extracellular polymeric substance (EPS) matrix, and that both the EPS (polysaccharides, proteins, and nucleic acids) and cell walls of *L. casei* contain polysaccharides (*32*, *33*). Thus, macrophages that encounter *L. casei* can be easily stimulated by the exposed polysaccharides of *L. casei* biofilms.

Considering the above-mentioned polysaccharide component of bacterial biofilm, we proposed that *L. casei* biofilms can stimulate macrophages to secrete osteogenic factors and enhance osteogenic differentiation of mesenchymal stem cells (MSCs). Here, the *L. casei* was chosen as a safe probiotics-based agent to modify the surface of Ti implants. *L. casei* biofilms were cultured on the surface of alkali heat–treated Ti substrates and then inactivated by ultraviolet (UV) irradiation to prevent colonization by viable bacteria. As the active ingredient of *L. casei* biofilms persists after short-term UV irradiation, we expected that an inactivated *L. casei* biofilm might prevent MRSA infection and improve bone tissue regeneration simultaneously (Fig. 1A).

RESULTS

Characterization and antibacterial performance of *L. casei* biofilm

The preparation procedure of *L. casei* biofilm–modified implants is shown in fig. S1A. The Ti implant was first treated with alkali heat treatment (AHT) to change the flat structure of the Ti surface and increase its roughness. *L. casei* was then cultured on the surface of AHT-Ti for 3 days to form a biofilm, followed by inactivation of the *L. casei* biofilm using a UV irradiation. As shown in fig. S1B, after AHT, the surface of AHT-Ti exhibited a three-dimensional network structure compared with the flat structure of the untreated Ti. These two samples were then cultured with *L. casei* for 3 days, respectively. In fig. S1C, it can be observed that the sparse *L. casei* were dispersed on the Ti surface. In contrast, the dense *L. casei* were spread on the surface of AHT-Ti, indicating that the three-dimensional network structure might provide more anchor points for the bacteria to adhere (Fig. 1B). In addition, the cell membrane of *L. casei* showed obvious wrinkling due to the damage brought by the intensive UV irradiation. To further investigate the viability of the *L. casei* treated by UV, the Live/Dead (green/red) staining assay was performed. As shown in Fig. 1C and fig. S1C, all of the adhered *L. casei* showed red fluorescence, suggesting that the *L. casei* on the surface of samples were successfully inactivated. From the section image of
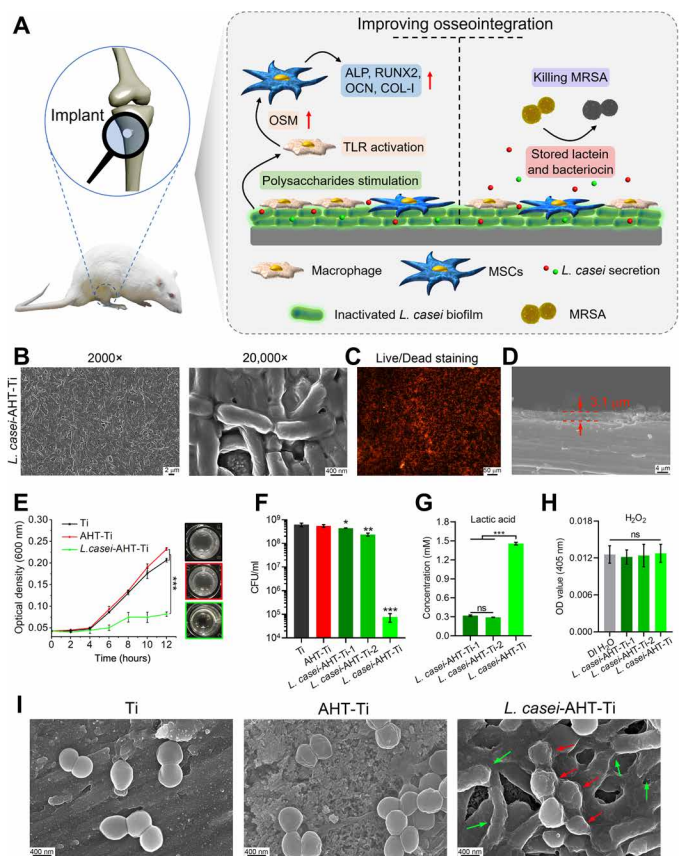

Fig. 1. Characterization and antibacterial performance of *L. casei* biofilm. (**A**) General concept of using inactivated *L. casei* biofilm to prevent MRSA infection and improve bone tissue regeneration simultaneously. (**B**) Surface morphology of *L. casei* biofilm–modified AHT-Ti. (**C**) Live/dead (green/red) staining of *L. casei* biofilm–modified AHT-Ti. (**D**) Section image of *L. casei*-AHT-Ti. (**E**) Growth of MRSA on the surface of Ti, AHT-Ti, and *L. casei*-AHT-Ti and corresponding photos of bacteria solution after 12 hours (right). Photo credit: L.T., Hubei University. (**F**) Number of MRSA colonies in the groups of Ti, AHT-Ti, *L. casei*-AHT-Ti-1 (1 day), *L. casei*-AHT-Ti-2 (2 days), and *L. casei*-AHT-Ti (3 days). (**G**) Lactic acid and (**H**) H_2O_2 detections from *L. casei*-AHT-Ti-1, *L. casei*-AHT-Ti-2, and *L. casei*-AHT-Ti with different culture time of biofilm. (**I**) SEM images of bacteria on the surface of samples. $n = 3$ independent experiments per group, *$P < 0.05$, **$P < 0.01$, and ***$P < 0.001$. ns, not significant.

L. casei-AHT-Ti, the thickness of biofilm was around 3.1 μm, indicating that the biofilm was consisted of about two layers of *L. casei* (Fig. 1D). The *L. casei* was obtained from the biofilm by scratching and ultrasonication, and their counts were investigated through spread plate method. The bacterial colonies on the surface of Ti and AHT-Ti (disc, diameter = 6 mm) were calculated to be 3.9×10^4 colony-forming units (CFUs) and 4.6×10^6 CFU, respectively, which further confirmed that more *L. casei* were adhered on the surface of AHT-Ti (fig. S1D). The contents of N and Ti elements detected by x-ray photoelectron spectroscopy (XPS) were increased and decreased, respectively, due to the coverage of *L. casei* biofilm (fig. S1E). In addition, from the scanning electron microscopy (SEM) images of *L. casei*-AHT-Ti (fig. S2), the *L. casei* biofilm adhered on the surface of Ti-AHT did not show notable change even after immersing in phosphate-buffered saline (PBS) solution for 7, 14, and 28 days, suggesting that the adhered biofilm was very stable. To investigate the mechanical stability of the biofilm coating on the

surface of implants, the surface of *L. casei*-AHT-Ti was scratched by a 200-µl pipette tip and a 5-ml syringe needle, respectively. As shown in fig. S3, when the biofilm was scratched by the pipette tip, it could be observed that the substrate was still covered with *L. casei*. As for the syringe needle, the substrate could be seen after scratching, but the edge of scratch was smooth without peeling. These results proved that the prepared *L. casei* biofilm had a good mechanical stability.

MRSA was chosen for testing the antibacterial ability of *L. casei*-AHT-Ti. Two hundred microliters of MRSA (1×10^6 CFU/ml) was cultured with each sample for 12 hours. Every 2 hours, the optical density (OD) value of bacteria solution was measured until 12 hours. As shown in Fig. 1E, the OD curves showed that the growth of MRSA was significantly inhibited from 0.04 to 0.08 in the group of *L. casei*-AHT-Ti, while the OD value in the groups of Ti and AHT-Ti increased from 0.04 to 0.21 and 0.23 after 12 hours, respectively. The corresponding photos of bacteria solution in 96-well plates showed that the solution in the *L. casei*-AHT-Ti was much clearer than the other two groups. Furthermore, from the spread plate results, the number of bacterial colonies in the *L. casei*-AHT-Ti showed more than three magnitudes reduction with an antibacterial efficiency of 99.98%. Besides, the *L. casei* biofilm cultured for 1 (*L. casei*-AHT-Ti-1) or 2 (*L. casei*-AHT-Ti-2) days showed weak antibacterial performance, which might be due to their less production of antibacterial secretion (Fig. 1F). As mentioned above, bacteriocin, lactic acid, and hydrogen peroxide are the main antibacterial components of *L. casei*. Thus, these components of *L. casei*-AHT-Ti-1, *L. casei*-AHT-Ti-2, and *L. casei*-AHT-Ti were tested. As shown in Fig. 1G, the concentration of lactic acid was measured to be 1.46 mM in *L. casei*-AHT-Ti for antibacterial environment, which was much higher than that of the groups of *L. casei*-AHT-Ti-1 and *L. casei*-AHT-Ti-2. However, the content of H_2O_2 in all biofilm showed no significant difference with deionized (DI) H_2O group, suggesting that its content was very little because the produced H_2O_2 was washed away by DI H_2O in the preparation step (Fig. 1H). The secretion of bacteriocin with a molecular weight about 5 kDa was measured by a tricine-SDS-PAGE (polyacrylamide gel electrophoresis) technique (*22*). It was found that the highest amount of bacteriocin was produced in *L. casei*-AHT-Ti when the biofilm was cultured for 3 days compared with 1- and 2-day cultivation (fig. S4). The above results showed that enough amount of lactic acid and bacteriocin could be produced from *L. casei* biofilm with 3 day's culture to kill MRSA efficiently. From the SEM images of bacteria (Fig. 1I), the cell walls of MRSA on the surface of Ti and AHT-Ti still kept intact, whereas both the cell walls of MRSA and *L. casei* on the surface of *L. casei*-AHT-Ti showed serious damage (indicated by red and green arrows), suggesting that even the inactivated *L. casei* also could kill MRSA due to the stored antibacterial components, including lactic acid and bacteriocin in the *L. casei* biofilm. These results indicated that the inactivated *L. casei* biofilm could endow the implant with excellent antibacterial performance.

Activation of macrophages by *L. casei* biofilm
The key hypothesis of our study is that the macrophages could be activated by the *L. casei* biofilm on the surface of implant to enhance osteogenic differentiation of MSCs through immunoregulation. Therefore, after confirming the antibacterial ability of *L. casei*-AHT-Ti, we next investigated the influence of *L. casei* biofilm on the modulation of macrophages. We stained the macrophages on the surface

of Ti, AHT-Ti, and *L. casei*-AHT-Ti by 4′,6-diamidino-2-phenylindole (nucleus) and fluorescein isothiocyanate (FITC)–conjugated phalloidin (F-actin) to observe their morphologies. As shown in Fig. 2A, the macrophages showed normal morphologies and assembled properly on the surface of all samples. The number of macrophages did not show an obvious decrease in the presence of *L. casei* after 48-hour coculture. The enhanced cell viability of macrophages on AHT-Ti after 24-hour coculture might be due to the fact that the three-dimensional network structure increased the initial adhesion of macrophages. However, the cell viability of macrophages in the three groups did not exhibit much difference after 48-hour coculture (Fig. 2B). These results suggested that the *L. casei* biofilm had no cytotoxicity to macrophages. Recent studies showed that the polysaccharides could stimulate macrophages through Toll-like receptor (TLR) activation to secrete osteoinductive cytokines such as oncostatin M (*OSM*) to improve osteogenesis (*31*). Thus, we first measured the gene expression of *OSM*, tumor necrosis factor–α (*TNF*-α), and interleukin-10 (*IL-10*) because of the fact that the *OSM* is a known cytokine to induce osteogenesis and the other two are typical proinflammatory and anti-inflammatory factors, respectively. From the reverse transcription polymerase chain reaction (RT-PCR) results (Fig. 2, C to E), the *OSM* expression was obviously increased (3.4-fold versus control) while the groups of AHT-Ti showed no significant difference from Ti, suggesting that only the *L. casei* biofilm on the surface of implants could improve the secretion of *OSM* but not the three-dimensional network structure of AHT-Ti. We found that the expressions of *TNF*-α (2.4-fold versus control) and *IL-10* (4.7-fold versus control) were enhanced in the group of *L. casei*-AHT-Ti, indicating that both of the proinflammatory and anti-inflammatory cytokines were produced through *L. casei* biofilm stimulation. Whether M1 or M2 macrophage polarization, it was reported that both of them could improve osteogenic differentiation of osteoblast (*34, 35*). However, a prolonged M1 activation may lead to extensive inflammatory responses and fibrosis of the implants. So, the polarization of macrophages was further studied by flow cytometry test after 2 and 3 days of treatment. Before treatment, the original status of the macrophages was proved to be M0 phenotypes through the characterization of macrophages phenotypes via CD11b, F4/80, CD11c, and CD206 (fig. S5). As shown in Fig. 2F, the macrophages showed increased CD11c (M1 marker) expression in *L. casei*-AHT-Ti compared with those in Ti and AHT-Ti groups, suggesting M1-type macrophages on day 2. However, the decreased expression of CD11c and the highest CD206 (M2 marker) were observed in *L. casei*-AHT-Ti, indicating that the macrophages shifted toward the M2 phenotype on day 3. In addition, *TNF*-α and *IL-10* in *L. casei*-AHT-Ti exhibited notably decreased and increased expression, respectively, compared with the Ti group, suggesting that the process of M1 polarization was not prolonged and would not lead to extensive inflammatory responses (fig. S6), which was in line with the results of flow cytometry. This phenomenon might be because the growing macrophages could not continue to contact with the polysaccharides of biofilm due to the coverage of the initial macrophages. Besides, the potential anti-inflammatory ability of *L. casei* also contributed to avoiding the overactive M1 polarization (*15*). To deeply study the immunoregulation mechanism of *L. casei* to macrophage, we next performed transcriptomics analysis of macrophages cultured on the Ti (control) and *L. casei*-AHT-Ti groups for 2 days. From the detected 55,536 genes, the samples between Ti (control) and *L. casei*-AHT-Ti were obviously separated by applying principal
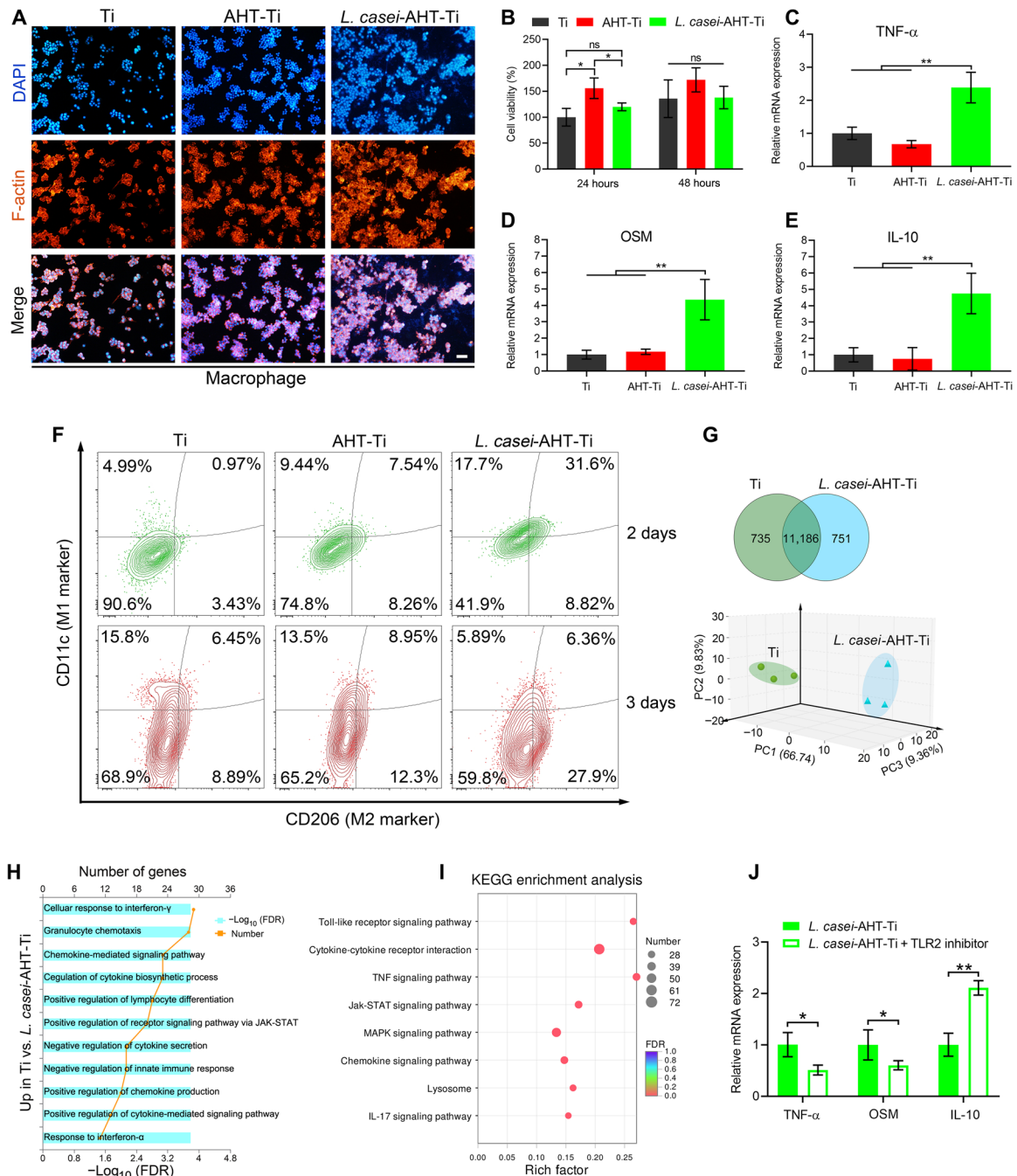
Fig. 2. Activation of macrophages by *L. casei*-AHT-Ti. (**A**) Macrophages in the presence of Ti, AHT-Ti, and *L. casei*-AHT-Ti were stained by 4′,6-diamidino-2-phenylindole (DAPI; nucleus) and FITC-conjugated phalloidin (F-actin). Scale bar, 50 μm. (**B**) Cell viability of macrophages. Gene expression of (**C**) *TNF*-α, (**D**) *OSM*, and (**E**) *IL-10*. (**F**) Flow cytometry results of CD11c (M1 marker) and CD206 (M2 marker) expression (gated on CD11b⁺) after 2 and 3 days of treatments. (**G**) Venn diagram of differentially expressed genes treated by Ti and *L. casei*-AHT-Ti (top) and PCA plot shows the obvious separation gene expression of macrophages (bottom). (**H**) Up-regulated GO 514 enrichment analysis in *L. casei*-AHT-Ti compared with Ti. FDR, false discovery rate; JAK, Janus kinase; STAT, signal transducer and activator of transcription. (**I**) KEGG pathway analysis of the identified different gene expression. MAPK, mitogen-activated protein kinase. (**J**) Gene expression of *TNF*-α, *OSM*, and *IL-10* in the presence of TLR2 inhibitor. $n = 3$ independent experiments per group, $*P < 0.05$ and $**P < 0.01$.

components analysis (PCA), indicating the significant transcriptome reprogramming in response to *L. casei*. The two groups had many changes (735 genes in Ti and 751 genes in *L. casei*-AHT-Ti), and they shared 11,186 genes (Fig. 2G). According to the gene ontology (GO) enrichment analysis, it was found that 215 genes were up-regulated

in *L. casei*-AHT-Ti, which was correlated with regulation of the cellular response to interferon-γ, granulocyte chemotaxis, chemokine-mediated signaling pathway, regulation of cytokine biosynthetic processes, positive regulation of lymphocyte differentiation, and positive regulation of receptor signaling pathway via Janus kinase–signal transducers and

activators of transcription, etc. Among the GO enrichment, the main up-regulated genes were rich in binding activity, chemokine, and cytokine secretion of macrophages due to the TLR activation of macrophages by *L. casei* (Fig. 2H and fig. S7). Kyoto Encyclopedia of Genes and Genomes (KEGG) pathway analysis showed the comprehensive immunoreaction of macrophages, indicating the mainly activated signaling pathway including TLR signaling pathway, cytokine-cytokine receptor interaction, and TNF signaling pathway (Fig. 2I). These activated signaling pathways could result in the M1 macrophage development referred to in the previous studies (*36*). To further prove the TLR activation in macrophage and its relationship with the increase of cytokine, a TLR2 inhibitor was chosen to treat the group of *L. casei*-AHT-Ti. As shown in Fig. 2J, when the macrophages were treated by TLR2 inhibitor, the expressions of both *TNF-α* and *OSM* decreased obviously due to the block of TLR2 signaling, which further proved the activation of TLR in macrophages. The increased expression of *IL-10* might be due to the inhibition of M1 polarization by TLR2 inhibitor.

Generation of osteoinductive cytokines by macrophages

To further analyze the secretion of macrophages activated by *L. casei*, the expression change of chemokines, cytokines, and growth factors between two samples were singled out and illustrated in Fig. 3A. From the heatmap of secreted factors, we found that the genes of *IL-1b*, *IL-6*, *OSM*, leukemia inhibitory factor (*LIF*), *IL-10*, *TNF-α*, vascular endothelial growth factor A (*VEGFA*), colony stimulating factor 3 (*CSF3*), fibroblast growth factor 2 (*FGF2*), bone morphogentic protein 6 (*BMP6*), cyclooxygenase 14 (*COX14*), *Wnt7b*, and *Wnt6*

were up-regulated in the group of *L. casei*-AHT-Ti. Their expressions were associated with osteoblasts differentiation. Besides, the up-regulated *IL-1b*, *IL-6*, and *TNF-α* were attributed to the proinflammatory signals, suggesting that the *L. casei* enhanced the activation of M1 macrophages. The anti-inflammatory cytokine of *IL-10* was up-regulated for *L. casei*–modified implants, which could inhibit the excessive inflammatory response (*37*, *38*). As a member of *IL-6* family, *OSM* is a potent inducer for enhancing osteoblasts differentiation, which was also obviously up-regulated. Since the COX2 (cyclooxygenase 2)–PGE$_2$ (prostaglandin E$_2$) pathway determines the production of *OSM* (*29*), the corresponding gene expressions were also investigated. As shown in Fig. 3B, besides the up-regulation of *OSM*, *IL-6*, *TNF-α*, and *IL-1b*, the expressions of *CD14* (lipopolysaccharide receptor), *COX2*, and E-series of prostaglandin receptor (*EPR*) were also up-regulated, which further proved the increased production of *OSM*. Besides, the activated COX2-PGE$_2$ pathway improved the expression of *OSM*. The protein levels of CD14, COX2, PGE$_2$, EPR, OSM, IL-6, TNF-α, IL-1β, and IL-10 were further quantified by enzyme-linked immunosorbent assay (ELISA). In Fig. 3C, the expressions of the above proteins in *L. casei*-AHT-Ti group were all higher than those in Ti group after 48 hours, which was consistent with the above results. From the above results, the complete process of macrophages activated by *L. casei*-AHT-Ti for further stimulating osteogenesis was illustrated in Fig. 3D. First, the *L. casei* biofilm on the surface of *L. casei*-AHT-Ti contacted with the CD14 of macrophages through the polysaccharides of biofilm, which could be proved by the activated TLR signaling pathway. Then, the CD14 activated the TLR2 to boost the M1 macrophages
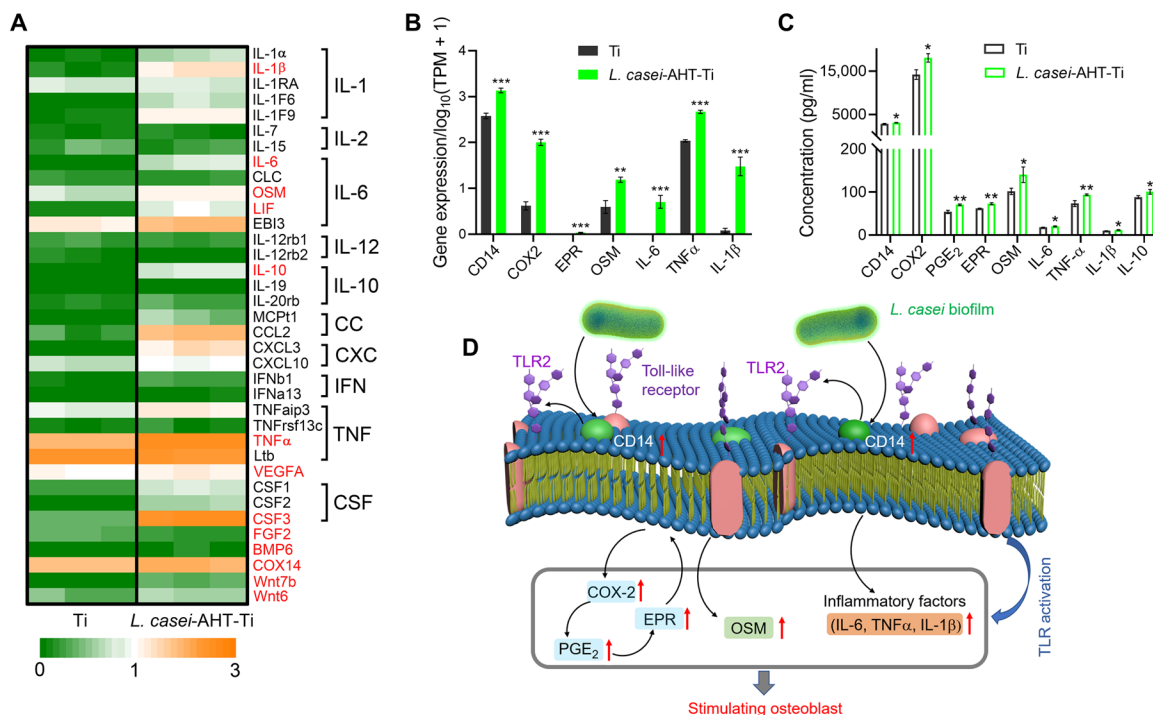
Fig. 3. Generation of osteoinductive cytokines by macrophages. (**A**) Expression change of the singled-out chemokines, cytokines, and growth factors between Ti and *L. casei*-AHT-Ti. (**B**) Expression of genes related to the production of *OSM* including *CD14* (lipopolysaccharide receptor), *COX2*, and *EPR*. (**C**) Protein levels of CD14, COX2, PGE$_2$, EPR, OSM, IL-6, TNF-α, IL-1β, and IL-10 were further quantified by ELISA assay. (**D**) Complete process of macrophage activated by *L. casei*-AHT-Ti for further stimulating osteogenesis. *n* = 3 independent experiments per group, Ti versus *L. casei*-AHT-Ti, *P < 0.05, **P < 0.01, and ***P < 0.001. IFN, interferon.

phenotype and enhance the production of proinflammatory factors including IL-6, TNF-α, and IL-1β. The stimulation of macrophages was expected to further regulate the MSCs differentiation.

Osteogenic differentiation of MSCs

In Fig. 4A, the MSCs adhered on the surface of *L. casei*-AHT-Ti spread as well as those on the groups of Ti and AHT-Ti. Besides, the cell viability of MSCs showed not much difference in these samples at days 1, 3, 7, and 14, which proved that the inactivated *L. casei* biofilm exhibited an excellent cytocompatibility to MSCs after long-term culture (Fig. 4B). Considering that the macrophages could secrete cytokine to induce osteogenesis, the culture solutions of macrophages (CM) treated by Ti, AHT-Ti, and *L. casei*-AHT-Ti were collected and incubated with MSCs separately. The alkaline phosphatase (ALP) activity was measured with an ALP kit after 14 days of culture. As shown in Fig. 4C, the ALP activity of CM$^{L.\ casei\text{-}AHT\text{-}Ti}$ was higher than that of both CM^{Ti} and CM$^{AHT\text{-}Ti}$ groups. We further tested the osteogenic-related gene expression of *ALP*, runt-related transcription factor 2 (*RUNX2*), osteocalcin (*OCN*), and type I collagen (*COL-I*) after 14 days. From the RT-PCR results (Fig. 4D), the expressions of ALP, RUNX2, OCN, and COL-I in the CM$^{L.\ casei\text{-}AHT\text{-}Ti}$ maintained the highest level in all samples. The calcium deposition of samples was stained by Alizarin red. In Fig. 4 (E and F), it could be obviously observed that the CM$^{L.\ casei\text{-}AHT\text{-}Ti}$ induce the highest matrix mineralization. These results demonstrated that the activated macrophages by *L. casei* biofilm successfully improved the osteogenic differentiation of MSCs in vitro.

Bone integration of *L. casei*-AHT-Ti in vivo

Next, we investigated the bone integration ability of *L. casei*-AHT-Ti in vivo (*n* = 3 per group). Without MRSA infection, it could be observed from the micro–computed tomography (micro-CT) results that the amount of new bone tissue on the interface of bone-implant in the *L. casei*-AHT-Ti group was more than that in the groups of Ti and AHT-Ti, so did the trabecular bone around the implants. The bone volume (BV)/tissue volume (TV) values of Ti, AHT-Ti, and *L. casei*-AHT-Ti were calculated to be 16.08, 20.68, and 26.89%, respectively (fig. S8, A and B), indicating that the *L. casei* biofilm could improve osseointegration of Ti implant in vivo. The immuno-histochemical staining of inducible nitric oxide synthase (iNOS) (M1) and transforming growth factor–β (TGFβ; M2) for macrophages around the implanted tissue showed that the macrophages exhibited the lowest M1 polarization and the most M2 polarization in the *L. casei*-AHT-Ti group after 4 weeks of implantation, suggesting that the *L. casei*-AHT-Ti could improve bone tissue regeneration and had the lowest inflammatory response (fig. S8, C to E). Since the pathogenic infections often occur during the implantation, to study the bone integration in the presence of pathogenic bacteria, we implanted the samples adhered with MRSA into the tibial plateaus of rats. Hematoxylin and eosin (H&E) and Giemsa staining were performed after 14-day implantation to investigate the inflammatory response and the remaining bacteria in the bone tissue around the implant. As shown in Fig. 5A, it could be observed that lots of inflammatory cells including neutrophil, lymphocyte, and monocytes infiltrated into the tissues around Ti and AHT-Ti implants. In contrast, fewer inflammatory cells were found in the *L. casei*-AHT-Ti, indicating the relief of inflammation reaction. In addition, the remaining MRSA was decreased significantly, suggesting that the *L. casei* biofilm also could kill MRSA in vivo and eliminate the infection without introducing severe inflammation reaction. To investigate the
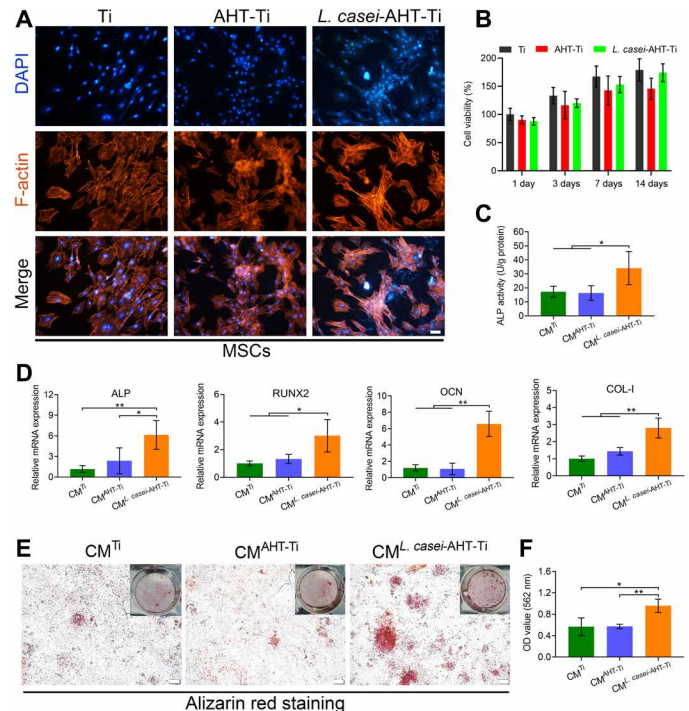

Fig. 4. Osteogenic differentiation of MSCs. (**A**) Cell morphology of MSCs in the presence of Ti, AHT-Ti, and *L. casei*-AHT-Ti. Scale bar, 50 μm. (**B**) Cell viability of MSCs. (**C**) ALP activity of MSCs in the groups of Ti, AHT-Ti, and *L. casei*-AHT-Ti after 14 days. (**D**) Osteogenic-related gene expression of ALP, RUNX2, and OCN after 14 days. (**E**) Alizarin red staining of samples after 14 days. Scale bars, 200 μm. Photo credit: L.T., Hubei University. (**F**) Quantification of the Alizarin red staining intensity. *n* = 3 independent experiments per group, *P < 0.05 and **P < 0.01.

antibacterial efficiency of *L. casei*-AHT-Ti toward MRSA in vivo, the implants were pulled out after 12-hour implantation and then rolled on the agar plates and cultured for another 24 hours. As shown in Fig. 5B, compared with the densely distributed colonies in the Ti and AHT-Ti groups, only several bacterial colonies were observed in the *L. casei*-AHT-Ti. The antibacterial efficiency of *L. casei*-AHT-Ti compared with Ti was calculated to be 98.1%, suggesting the excellent antibacterial performance of *L. casei*-AHT-Ti in vivo (Fig. 5C). From the micro-CT results (Fig. 5D), it could be observed that the amount of new bone tissue on the interface of bone implant in the *L. casei*-AHT-Ti group was more than that in the groups of Ti and AHT-Ti, so did the trabecular bone around the implant. The BV/TV values of Ti, AHT-Ti, and *L. casei*-AHT-Ti were calculated to be 25.72, 26.4, and 34.64%, respectively (Fig. 5E). The details in the newly formed bone tissue at the bone-implant interface were further studied by Van Gieson's picrofuchsin staining (Fig. 5F). We clearly observed a large area of bone matrix (red stain) on the surface of the *L. casei* biofilm–modified Ti rods because the immunoactive *L. casei* film not only improved the osteogenic activities but also prevented the MRSA-associated infection. The bone area ratios of Ti, AHT-Ti, and *L. casei*-AHT-Ti were calculated to be 18.54, 18.68, and 27.92%, respectively (Fig. 5G). Less bone tissue was observed on the rods of Ti and AHT-Ti due to the lack of osteogenic activity and the occurrence of infection. The above in vivo results definitely proved that this engineered *L. casei* film could efficiently eradicate MRSA infection and improve the osseointegration of Ti implants simultaneously.
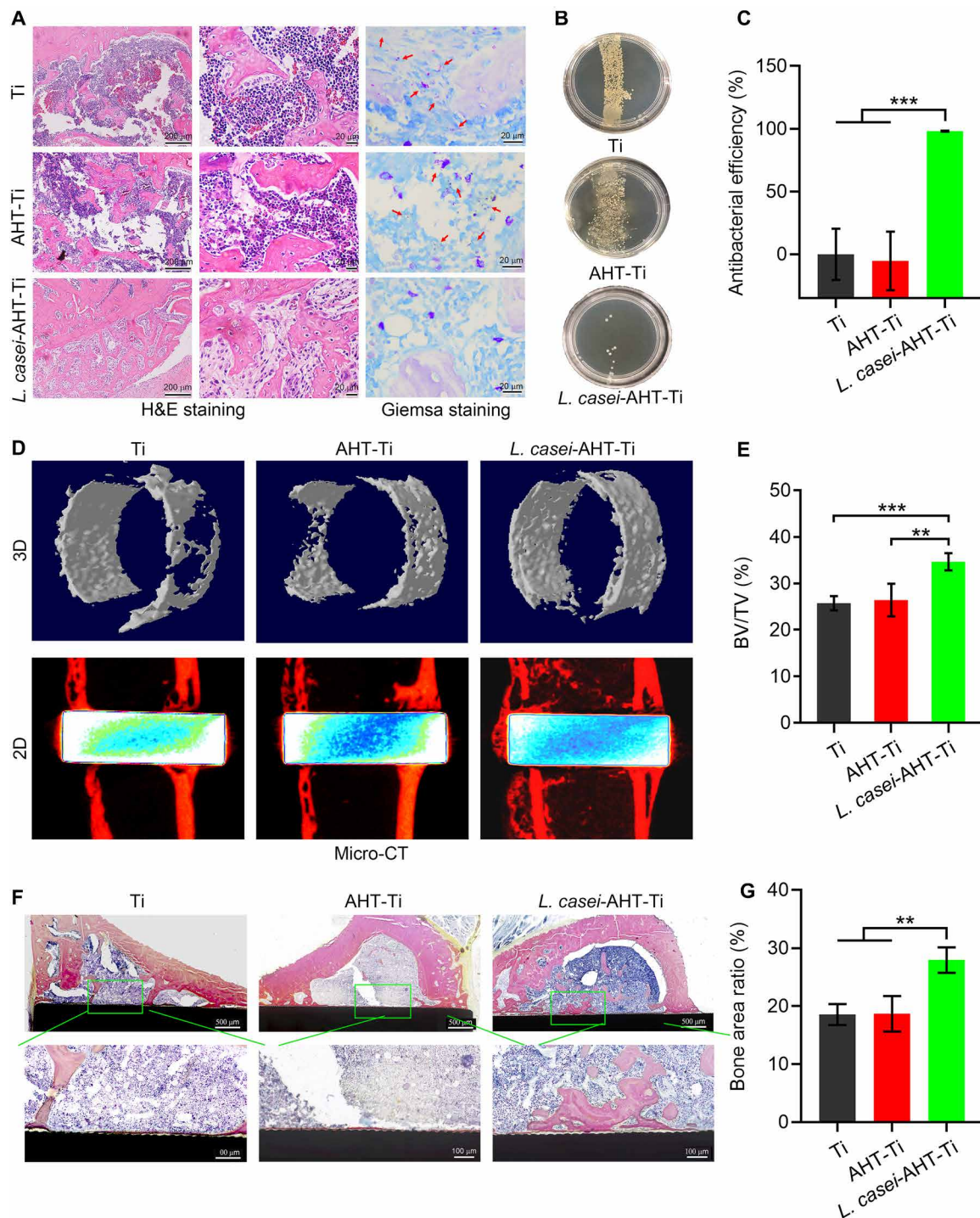
Fig. 5. Bone integration of *L. casei*-AHT-Ti in vivo. (**A**) H&E and Giemsa staining of bone tissue around the implants. (**B**) Remaining bacteria colonies of the Ti, AHT-Ti, and *L. casei*-AHT-Ti rods pulled out from the bone tissues. Photo credit: L.T., Hubei University. (**C**) Antibacterial efficiency of *L. casei*-AHT-Ti compared with Ti and AHT-Ti groups in vivo. (**D**) Micro-CT results. 3D, three-dimensional. (**E**) BV/TV values of Ti, AHT-Ti, and *L. casei*-AHT-Ti. (**F**) Van Gieson's picrofuchsin staining of the newly formed bone tissues at the bone-implant interface. (**G**) Bone area ratios of samples calculated from the Van Gieson's picrofuchsin staining. $n = 3$ independent experiments per group, $**P < 0.01$ and $***P < 0.001$.

DISCUSSION

In summary, we have demonstrated the potential for use of engineered probiotics biofilms to prevent MRSA infection of implants and to improve bone integration between implants and surrounding tissues. The food-grade, inactivated *L. casei* biofilms exhibited excellent antibacterial performance toward MRSA both in vitro and in vivo due to their lactic acid and bacteriocin content. We found that this inactivated *L. casei* biofilm can activate the TLR signaling

pathway in macrophages to increase the production of OSM through contact between the polysaccharides of *L. casei* biofilms and lipo-polysaccharide receptors of macrophages. The secreted osteogenic cytokines successfully improved the osteogenic differentiation of MSCs and accelerated bone integration. The employment of inactivated probiotics modification without genetic engineering or introducing live bacteria into the blood will enable translation of this method to the clinical context. Because of their safety, engineered probiotics bio-films can be combined with biomaterials such as tissue engineering scaffolds or nanoparticles to endow them with diverse biological func-tions. We believe that probiotics are not only useful for treatments of intestinal diseases but also have potential application for immuno-therapy of other diseases.

METHODS

AHT of Ti substrates (AHT-Ti)
Medical Ti plates were polished with SiC sandpaper (#240, #800, and #1200) successively and washed with ethanol and DI water by ultrasonication, respectively. The polished Ti plates were then im-mersed into 4 M NaOH solution and heated at 80°C for 1.5 hours. After cooling, the samples were washed ultrasonically with ethanol and DI water, respectively, before use.

Preparation of *L. casei*-AHT-Ti
L. casei [200 μl, 10^8 CFU/ml; China Center for type Culture Collection (CCTCC) AB 2013355] was cultured with AHT-Ti in 96-well plates for 1, 2, and 3 days, respectively, and the culture medium was replaced with fresh culture medium containing *L. casei* (200 μl, 10^8 CFU/ml) every day. The samples were washed with DI water and dried. The *L. casei* biofilm on the surface of AHT-Ti was inactivated through UV irradiation for 1 hour.

Characterization
The surface morphology of samples was observed by field-emission SEM (ZEISS Sigma 500) and SEM (JSM-6510LV). The surface elemen-tal composition of samples was tested by an XPS (ESCALAB250Xi, Thermo Fisher Scientific, USA). The fluorescence of bacteria or os-teoblast cells on the surface of samples was observed by an inverted fluorescence microscope (IFM; Olympus, IX73, Japan).

In vitro antibacterial assay
MRSA (200 μl, 1×10^6 CFU/ml; CCTCC AB 2015108) was cultured with Ti, AHT-Ti, and *L. casei*-AHT-Ti groups at 37°C for 12 hours. The OD of bacterial solution at 600 nm was recorded every 2 hours, and the bacterial solution was taken out after 12 hours and diluted to spread on the surface of luria-bertani agar plates. After 24-hour incubation at 37°C, the CFUs were counted. The antibacterial efficiency was obtained according to the following equation: antibacterial effi-ciency (%) = $[(A - B)/A] \times 100\%$, in which A is the mean number of bacteria colonies on the Ti, and B is the mean number of bacteria colonies on the experimental groups. The MRSAs attached on the surface of samples were fixed with glutaraldehyde (2.5%) for 2 hours and washed with PBS solution. Before SEM observation, a gradient ethanol solution [30, 50, 70, 90, and 100% (v/v)] was added to dehydrate the samples for 15 min, respectively. The amounts of lactic acid and H_2O_2 in biofilm were measured by lactic acid and H_2O_2 kits, respectively (Nanjing Jiancheng Bioengineering Institute). The secretion of bac-teriocin was measured by a tricine–SDS-PAGE technique (*22*).

In vitro cytotoxicity assay
The MSCs at three passages and murine bone marrow–derived macrophages were obtained from Tongji Hospital in Wuhan, China. The macrophages (1×10^4 cells per well) cultured with Ti, AHT-Ti, and *L. casei*-AHT-Ti were incubated in Dulbecco's modified Eagle's medium supplemented with 10% (v/v) fetal bovine serum (FBS) and 1% penicillin-amphotericin for 24 or 48 hours. The MSCs (2.5×10^4 cells per well) were cultured with Ti, AHT-Ti, and *L. casei*-AHT-Ti in a growth medium containing F12, FBS, and penicillin-streptomycin for 1, 3, 7, and 14 days. After that, the MTT [3-(4,5-dimethylthiazol-2-yl)-2,5-diphenyltetrazolium bromide, 0.5 mg/ml; Aladdin Reagent Co., China] solution was added and incubated for 4 hours. The solution was removed, and 250 μl of dimethyl sulfoxide (DMSO) was added into each well. The OD value at 570 nm of DMSO solution was measured through a microplate reader (SpectraMax I3MD, USA) to evaluate the viability of cells.

Cell morphology
The MSCs and macrophages were cultured on the surface of sam-ples for 24 and 48 hours, respectively. Before staining, the cells were fixed with 4% formaldehyde and washed with PBS for two times. Then, the cells were stained by 4′,6-diamidino-2-phenylindole (nucleus, YiSen, Shanghai) and FITC-conjugated phalloidin (actin, YiSen, Shanghai) for 30 min, respectively. The cell morphology of MSCs and macrophages was observed by the IFM.

Transcriptome sequencing and data analysis
Macrophages (1×10^5 cells per well) were cultured with Ti and *L. casei*-AHT-Ti for 48 hours, respectively. Then, the macrophages were treated by TRIzol reagent (Beyotime Biotechnology) and stored at −80°C before sequencing. The RNA sequencing was per-formed using Illumina HiSeq X10 (Illumina, USA). The value of gene expression was transformed as $\log_{10}$[TPM (Transcripts Per Million reads) + 1]. The RNA sequencing data were normalized through fragments per kilobases per million reads method. The GO and KEGG pathway enrichment analysis were performed using the free online platform of Majorbio Cloud Platform (www.majorbio.com).

Quantitative PCR assay
The macrophages (1×10^5 cells per well) were cultured with Ti, AHT-Ti, and *L. casei*-AHT-Ti for 48 or 72 hours. The MSCs (1×10^5 cells per well) were treated by the CM treated by Ti, AHT-Ti, and *L. casei*-AHT-Ti (48 hours) for 14 days, respectively, and the corre-sponding groups were set as CM^{Ti}, CM^{AHT-Ti}, and $CM^{L.\ casei-AHT-Ti}$. The culture medium was changed every 2 days. The total RNA was extracted and reversely transcribed to complementary DNA by a PrimeScript RT Master Mix. RT-PCR analysis was examined using a Bio-Rad RT-PCR system. The gene expressions of *OSM*, *IL-10*, and *TNF*-α from macrophages were tested with or without TLR2 inhibitor (Invivogen). The osteogenesis-related gene expressions of *OCN*, *RUNX2*, *ALP*, and *COL-I* from MSCs were tested. The glyceraldehyde-3-phosphate dehydrogenase was used as the internal reference. Table S1 shows the primer sequences of the tested genes.

Flow cytometry analysis
To investigate the phenotypes of macrophages before experi-ment, Raw264.7 cells were collected with 0.25% (v/v) trypsin-EDTA solution and centrifuged at 1500 rpm for 5 min. Thereafter, cells were incubated for 30 min in PBS containing fluorescently

labeled primary monoclonal antibodies [anti–CD11c-PE-CY[7], anti–CD11b-FITC, and anti–F4/80-PE (phycoerythrin)]. Then, the cells were washed with PBS and resuspended with 4% (v/v) formaldehyde for 15 min. After washing the cells three times with PBS, the cells were incubated for 30 min with anti–CD206–Alexa Fluor 647. After that, the cells were washed three times with PBS and resuspended with PBS for further analyzing using a flow cytometry (FACSCalibur). To study the phenotypes of macrophages during experiment, cells were blown and seeded in growth medium at a density of 1×10^5 cells per well. After 48- or 72-hour incubation, cells were collected with 0.25% (v/v) trypsin-EDTA solution and washed with PBS. Then, cells were incubated for 30 min in PBS containing fluorescently labeled primary monoclonal antibodies (anti–CD11c-PE-CY[7] and anti–CD11b-FITC). After being washed three times with PBS, the cells were fixed with 4% (v/v) formaldehyde for 15 min. After that, the cells were washed with PBS and incubated for 30 min with anti–CD206–Alexa Fluor 647. Then, the cells were washed three times with PBS and resuspended with PBS for further analyzing using a flow cytometry.

Enzyme-linked immunosorbent assay
The secretions of CD14, COX2, PGE$_2$, EPR, OSM, IL-6, TNF-α, IL-1β, and IL-10 from the macrophages cultured on Ti, AHT-Ti, and *L. casei*-AHT-Ti were measured by ELISA assay kits (Shanghai Enzyme-linked Biotechnology).

ALP activity assay
The MSCs (1×10^4 cells per well) were treated by the CM treated by of Ti, AHT-Ti, and *L. casei*-AHT-Ti (48 hours) for 14 days. Then, the MSCs were treated with 1% Triton X-100 solution. The culture medium was changed every 2 days. The ALP activity was measured using an ALP kit (Nanjing JianCheng Bioengineering Institute), and the total protein of MSCs was measured by a bicinchoninic acid assay kit (Solarbio).

Alizarin red staining
The matrix mineralization of samples was measured by Alizarin red staining. The MSCs (1×10^5 cells per well) were treated by osteogenic extracts medium [10^{-8} M dexamethasone, 10 mM β-glycerol phosphate, and ascorbic acid (50 μg/ml)] and the CM treated by Ti, AHT-Ti, and *L. casei*-AHT-Ti (48 hours) for 14 days, respectively. The culture medium was changed every 2 days. The MSCs were washed with PBS and fixed by 4% formaldehyde for 15 min. The fixed MSCs were stained by 1% Alizarin red (pH 4.2) for 5 min and washed with PBS five times.

Animals and surgical experiment
Male Sprague-Dawley rats (420 to 450 g) were obtained from Hubei Provincial Centers for Disease Prevention and Control, and the experimental protocols were approved by the animal research committee of the Tongji Medical College, Huazhong University of Science and Technology, Wuhan. The rods of Ti, AHT-Ti, and *L. casei*-AHT-Ti were coated with or without MRSA (1×10^6 CFU/ml, 20 μl) before implantation. In the surgery, the rats were anesthetized using pentobarbital [30 mg/kg, 1% (w/w)]. The samples were implanted into the tibial plateaus of the rats. For one batch, the rats were euthanized with overdose pentobarbital, and the corresponding rods were pulled out after 12-hour implantation. The rods were then rolled on the agar plates and cultured for another 24 hours. For another batch, the rats were euthanized after 4 weeks.

Histopathological and analysis
To investigate the inflammatory reaction, the bone tissues around the samples were harvested after 2-week implantation and then fixed with 4% paraformaldehyde, decalcified by EDTA, dehydrated in an ascending graded series of ethanol solutions, and embedded in paraffin. The tissues were stained by H&E and Giemsa staining to observe the inflammation level and the remaining bacteria. To investigate the bone integration situation around the implants, the bone tissue–contained implants were harvested after 4 weeks implantation. The samples were stained with Van Gieson's picrofuchsin staining. The macrophages in tissues were stained by iNOS and TGFβ.

Micro-CT analysis
The bone tissue–contained implants were scanned on a micro-CT system (SkyScan 1176, Bruker). Scans were reconstructed to generate three-dimensional digitized images. The BV/TV values were calculated by CT Analyser software (version 1.11; Skyscan).

Statistical analysis
All the results are presented as mean values ± SD with $n \geq 3$. A one-way analysis of variance (ANOVA) and Student's *t* test were used for significance analysis. *$P < 0.05$, **$P < 0.01$, and ***$P < 0.001$ were considered as statistically significant.

SUPPLEMENTARY MATERIALS
Supplementary material for this article is available at http://advances.sciencemag.org/cgi/content/full/6/46/eaba5723/DC1

View/request a protocol for this paper from *Bio-protocol*.

REFERENCES AND NOTES
1. J. Min, K. Y. Choi, E. C. Dreaden, R. F. Padera, R. D. Braatz, M. Spector, P. T. Hammond, Designer dual therapy nanolayered implant coatings eradicate biofilms and accelerate bone tissue repair. *ACS Nano* **10**, 4441–4450 (2016).
2. T. V. Nguyen, J. A. Eisman, P. J. Kelly, P. N. Sambrook, Risk factors for osteoporotic fractures in elderly men. *Am. J. Epidemiol.* **144**, 255–263 (1996).
3. B. P. Gupta, J. M. Huddleston, L. L. Kirkland, P. M. Huddleston, D. R. Larson, R. E. Gullerud, M. C. Burton, C. S. Rihal, R. S. Wright, Clinical presentation and outcome of perioperative myocardial infarction in the very elderly following hip fracture surgery. *J. Hosp. Med.* **7**, 713–716 (2012).
4. J. M. Huddleston, R. E. Gullerud, F. Smither, P. M. Huddleston, D. R. Larson, M. P. Phy, L. J. Melton III, V. L. Roger, Myocardial infarction after hip fracture repair: A population-based study. *J. Am. Geriatr. Soc.* **60**, 2020–2026 (2012).
5. J. M. A. Blair, M. A. Webber, A. J. Baylay, D. O. Ogbolu, L. J. V. Piddock, Molecular mechanisms of antibiotic resistance. *Nat. Rev. Microbiol.* **13**, 42–51 (2015).
6. M. Kather, M. Skischus, P. Kandt, A. Pich, G. Conrads, S. Neuss, Functional isoeugenol-modified nanogel coatings for the design of biointerfaces. *Angew. Chem. Int. Ed.* **56**, 2497–2502 (2017).
7. G. Jin, H. Qin, H. Cao, Y. Qiao, Y. Zhao, X. Peng, X. Zhang, X. Liu, P. K. Chu, Zn/Ag micro-galvanic couples formed on titanium and osseointegration effects in the presence of *S. aureus*. *Biomaterials* **65**, 22–31 (2015).
8. H. Cheng, W. Xiong, Z. Fang, H. Guan, W. Wu, Y. Li, Y. Zhang, M. M. Alvare, B. Gao, K. Huo, J. Xu, N. Xu, C. Zhang, J. Fu, A. Khademhosseini, F. Li, Strontium (Sr) and silver (Ag) loaded nanotubular structures with combined osteoinductive and antimicrobial activities. *Acta Biomater.* **31**, 388–400 (2016).
9. Y. Li, L. Liu, P. Wan, Z. Zhai, Z. Mao, Z. Ouyang, D. Yu, Q. Sun, L. Tan, L. Ren, Z. Zhu, Y. Hao, X. Qu, K. Yang, K. Dai, Biodegradable Mg-Cu alloy implants with antibacterial activity for the treatment of osteomyelitis: In vitro and in vivo evaluations. *Biomaterials* **106**, 250–263 (2016).
10. J. Li, L. Tan, X. Liu, Z. Cui, X. Yang, K. W. K. Yeung, P. K. Chu, S. Wu, Balancing bacteria–osteoblast competition through selective physical puncture and biofunctionalization

of ZnO/polydopamine/arginine-glycine-aspartic acid-cysteine nanorods. *ACS Nano* **11**, 11250–11263 (2017).

11. P. Liang, Q. Tang, Y. Cai, G. Liu, W. Si, J. Shao, W. Huang, Q. Zhang, X. Dong, Self-quenched ferrocenyl diketopyrrolopyrrole organic nanoparticles with amplifying photothermal effect for cancer therapy. *Chem. Sci.* **8**, 7457–7463 (2017).

12. S. Chowdhury, S. Castro, C. Coker, T. E. Hinchliffe, N. Arpaia, T. Danino, Programmable bacteria induce durable tumor regression and systemic antitumor immunity. *Nat. Med.* **25**, 1057–1063 (2019).

13. J. H. Zheng, V. H. Nguyen, S.-N. Jiang, S.-H. Park, W. Tan, S. H. Hong, M. G. Shin, I.-J. Chung, Y. Hong, H.-S. Bom, H. E. Choy, S. E. Lee, J. H. Rhee, J.-J. Min, Two-step enhanced cancer immunotherapy with engineered *Salmonella typhimurium* secreting heterologous flagellin. *Sci. Transl. Med.* **9**, eaak9537 (2017).

14. D.-W. Zheng, Y. Chen, Z.-H. Li, L. Xu, C.-X. Li, B. Li, J.-X. Fan, S.-X. Cheng, X.-Z. Zhang, Optically-controlled bacterial metabolite for cancer therapy. *Nat. Commun.* **9**, 1680 (2018).

15. M. G. Gareau, P. M. Sherman, W. A. Walker, Probiotics and the gut microbiota in intestinal health and disease. *Nat. Rev. Gastroenterol. Hepatol.* **7**, 503–514 (2010).

16. L. Steidler, W. Hans, L. Schotte, F. Neirynck, F. Obermeier, W. Falk, W. Fiers, E. Remaut, Treatment of murine colitis by *Lactococcus lactis* secreting interleukin-10. *Science* **289**, 1352–1355 (2000).

17. J. J. Hay, A. Rodrigo-Navarro, M. Petaroudi, A. V. Bryksin, A. J. García, T. H. Barker, M. J. Dalby, M. Salmeron-Sanchez, Bacteria-based materials for stem cell engineering. *Adv. Mater.* **30**, 1804310 (2018).

18. D. T. Riglar, P. A. Silver, Engineering bacteria for diagnostic and therapeutic applications. *Nat. Rev. Microbiol.* **16**, 214–225 (2018).

19. M. A. D. Groote, D. N. Frank, E. Dowell, M. P. Glode, N. R. Pace, *Lactobacillus rhamnosus* GG bacteremia associated with probiotic use in a child with short gut syndrome. *Pediatr. Infect. Dis. J.* **24**, 278–280 (2005).

20. R. E. Berger, *Lactobacillus* sepsis associated with probiotic therapy. *J. Urol.* **174**, 1843 (2005).

21. M. Peng, G. Reichmann, D. Biswas, *Lactobacillus casei* and its byproducts alter the virulence factors of foodborne bacterial pathogens. *J. Funct. Foods* **15**, 418–428 (2015).

22. M. Ghanbari, M. Jami, W. Kneifel, K. J. Domig, Antimicrobial activity and partial characterization of bacteriocins produced by *Lactobacilli* isolated from Sturgeon fish. *Food Control* **32**, 379–385 (2013).

23. V. L.-L. Moal, A. L. Servin, Anti-infective activities of *Lactobacillus* strains in the human intestinal microbiota: From probiotics to gastrointestinal anti-infectious biotherapeutic agents. *Clin. Microbiol. Rev.* **27**, 167–199 (2014).

24. T. R. Klaenhammer, M. Kleerebezem, M. V. Kopp, M. Rescigno, The impact of probiotics and prebiotics on the immune system. *Nat. Rev. Immunol.* **12**, 728–734 (2012).

25. J. M. Anderson, A. Rodriguez, D. T. Chang, Foreign body reaction to biomaterials. *Semin. Immunol.* **20**, 86–100 (2008).

26. Z. Chen, A. Bachhuka, S. Han, F. Wei, S. Lu, R. M. Visalakshan, K. Vasilev, Y. Xiao, Correction to "Tuning chemistry and topography of nanoengineered surfaces to manipulate immune response for bone regeneration applications". *ACS Nano* **13**, 3739–3739 (2019).

27. Y. Niu, Q. Li, R. Xie, S. Liu, R. Wang, P. Xing, Y. Shi, Y. Wang, L. Dong, C. Wang, Modulating the phenotype of host macrophages to enhance osteogenesis in MSC-laden hydrogels: Design of a glucomannan coating material. *Biomaterials* **139**, 39–55 (2017).

28. C. Wu, Y. Zhou, M. Xu, P. Han, L. Chen, J. Chang, Y. Xiao, Copper-containing mesoporous bioactive glass scaffolds with multifunctional properties of angiogenesis capacity, osteostimulation and antibacterial activity. *Biomaterials* **34**, 422–433 (2013).

29. P. Guihard, Y. Danger, B. Brounais, E. David, R. Brion, J. Delecrin, C. D. Richards, S. Chevalier, F. Rédini, D. Heymann, H. Gascan, F. Blanchard, Induction of osteogenesis in mesenchymal stem cells by activated monocytes/macrophages depends on oncostatin M signaling. *Stem Cells* **30**, 762–772 (2012).

30. S. Zamze, L. Martinez-Pomares, H. Jones, P. R. Taylor, R. J. Stillion, S. Gordon, S. Y. C. Wong, Recognition of bacterial capsular polysaccharides and lipopolysaccharides by the macrophage mannose receptor. *J. Biol. Chem.* **277**, 41613–41623 (2002).

31. Y. Shi, L. Wang, Y. Niu, N. Yu, P. Xing, L. Dong, C. Wang, Fungal component coating enhances titanium implant-bone integration. *Adv. Funct. Mater.* **28**, 1804483 (2018).

32. E. Yasuda, M. Serata, T. Sako, Suppressive effect on activation of macrophages by *Lactobacillus casei* strain shirota genes determining the synthesis of cell wall-associated polysaccharides. *Appl. Environ. Microbiol.* **74**, 4746–4755 (2008).

33. H. Koo, R. N. Allan, R. P. Howlin, P. Stoodley, L. Hall-Stoodley, Targeting microbial biofilms: Current and prospective therapeutic strategies. *Nat. Rev. Microbiol.* **15**, 740–755 (2017).

34. M. Shi, Z. Chen, S. Farnaghi, T. Friis, X. Mao, Y. Xiao, C. Wu, Copper-doped mesoporous silica nanospheres, a promising immunomodulatory agent for inducing osteogenesis. *Acta Biomater.* **30**, 334–344 (2016).

35. Y. Zhang, T. Böse, R. E. Unger, J. A. Jansen, C. J. Kirkpatrick, J. J. J. P. van den Beucken, Macrophage type modulates osteogenic differentiation of adipose tissue MSCs. *Cell Tissue Res.* **369**, 273–286 (2017).

36. R.-H. Deng, M.-Z. Zou, D. Zheng, S.-Y. Peng, W. Liu, X.-F. Bai, H.-S. Chen, Y. Sun, P.-H. Zhou, X.-Z. Zhang, Nanoparticles from cuttlefish ink inhibit tumor growth by synergizing immunotherapy and photothermal therapy. *ACS Nano* **13**, 8618–8629 (2019).

37. J. Li, W. Liu, D. Kilian, X. Zhang, M. Gelinsky, P. K. Chu, Bioinspired interface design modulates pathogen and immunocyte responses in biomaterial-centered infection combination therapy. *Mater. Horiz.* **6**, 1271–1282 (2019).

38. A. Eckhardt, T. Harorli, J. Limtanyakul, K.-A. Hiller, C. Bosl, C. Bolay, F.-X. Reichl, G. Schmalz, H. Schweikl, Inhibition of cytokine and surface antigen expression in LPS-stimulated murine macrophages by triethylene glycol dimethacrylate. *Biomaterials* **30**, 1665–1674 (2009).

Citation: L. Tan, J. Fu, F. Feng, X. Liu, Z. Cui, B. Li, Y. Han, Y. Zheng, K. W. K. Yeung, Z. Li, S. Zhu, Y. Liang, X. Feng, X. Wang, S. Wu, Engineered probiotics biofilm enhances osseointegration via immunoregulation and anti-infection. *Sci. Adv.* **6**, eaba5723 (2020).

ScienceAdvances

Engineered probiotics biofilm enhances osseointegration via immunoregulation and anti-infection

Lei TanJieni FuFan FengXiangmei LiuZhenduo CuiBo LiYong HanYufeng ZhengKelvin Wai Kwok YeungZhaoyang LiShengli ZhuYanqin LiangXiaobo FengXianbao WangShuilin Wu

View the article online
https://www.science.org/doi/10.1126/sciadv.aba5723
Permissions
https://www.science.org/help/reprints-and-permissions

Use of think article is subject to the Terms of service